Pergamon

Acta Materialia 50 (2002) 3057–3073

Acta MATERIALIA

www.actamat-journals.com

Computer simulation of 3-D grain growth using a phase-field model

C.E. Krill III [a,*], L.-Q. Chen [b]

[a] *FR 7.3 Technical Physics, Universität des Saarlandes, Postfach 151150, Geb. 43B, D-66041 Saarbrücken, Germany*
[b] *Department of Materials Science and Engineering, The Pennsylvania State University, University Park, PA 16802, USA*

Received 13 December 2001; received in revised form 18 February 2002; accepted 18 February 2002

Abstract

The kinetics and topology of grain growth in three dimensions are simulated using a phase-field model of an ideal polycrystal with uniform grain-boundary mobilities and energies. Through a dynamic grain-orientation-reassignment routine, the computational algorithm avoids grain growth via coalescence, thus eliminating the dependence of the simulation results on the number of order parameters implemented in the phase-field description of the polycrystalline microstructure. Consequently, far fewer order-parameter values must be computed than in previous formulations of the phase-field model, which permits handling simulation cells large enough to contain a statistically significant number of grains. The kinetic and topological properties of the microstructure induced by coarsening closely resemble those obtained by other methods for simulating coalescence-free grain growth in 3D. © 2002 Acta Materialia Inc. Published by Elsevier Science Ltd. All rights reserved.

Zusammenfassung

Die Kinetik und Topologie dreidimensionalen Kornwachstums werden mittels eines Phasenfeldmodells eines idealen Polykristalls mit uniformen Korngrenzenmobilitäten bzw. -energien simuliert. Mit Hilfe einer Routine zur dynamischen Zuordnung von Kornorientierungen vermeidet der Rechenalgorithmus das Auftreten von Kornwachstum durch Koaleszenz, so daß die Simulationsergebnisse nicht von der Anzahl der zur Phasenfeldbeschreibung der polykristallinen Mikrostruktur eingesetzten Ordnungsparameter abhängen. Infolgedessen müssen wesentlich weniger Ordnungsparameterwerte berechnet werden als in früheren Formulierungen des Phasenfeldmodells, was es gestattet, Simulationszellen zu behandeln, die groß genug sind, um eine statistisch signifikante Anzahl von Körnern zu beinhalten. Die kinetischen und topologischen Eigenschaften der durch Vergröberung induzierten Mikrostruktur ähneln denjenigen, die durch andere Methoden zur dreidimensionalen Simulierung koaleszensfreien Kornwachstums erhalten wurden. © 2002 Acta Materialia Inc. Published by Elsevier Science Ltd. All rights reserved.

Keywords: Computer simulation; Grain growth; Microstructure; Polycrystal

1. Introduction

Controlling the evolution of microstructure is crucial to the optimization of materials properties

* Corresponding author.
E-mail address: krill@rz.uni-sb-de (C.E. Krill III).

1359-6454/02/$22.00
PII: S1359-6454(02)00084-8

through processing. Consequently, it has been a primary goal of computational efforts in materials science to develop the capability to model microstructural transformations under realistic conditions with predictive accuracy [1]. To that end, a great deal of attention has been devoted to the technologically important phenomenon of grain growth in polycrystalline materials, which has been studied experimentally and theoretically for decades, yet has proven surprisingly difficult to model analytically [2,3]. In single-phase materials, the driving force for grain-boundary migration and the associated boundary mobility are reasonably well understood [4], suggesting that the coarsening of such systems should be amenable to a computational approach. In recent years, several techniques for the computer simulation of grain growth have been developed [5,6], including Monte Carlo Potts models [7,8], vertex tracking [9,10], front tracking [11,12], Voronoi tessellation [13,14], cellular automata [15] and phase-field approaches [16-22]. All of these methods were originally applied in two dimensions to the 'ideal' case of coarsening of a polycrystalline solid with uniform grain-boundary mobilities and energies. For such a system, the various computational models reach similar conclusions regarding the kinetic and topological aspects of 2-D grain growth, despite significant differences in underlying methodology [23,24].

With the availability of increasingly powerful computing facilities, it has recently become feasible to extend these grain-growth simulation algorithms to three dimensions—a prerequisite for meaningful comparison with experimental data recorded on bulk polycrystalline samples. The challenge upon doing so is to optimize the computational algorithm such that the coarsening of a statistically significant number of grains can be simulated under the constraints imposed by storage and computing-power limitations. This is usually a nontrivial task, as the memory and processing-time requirements needed to carry out a grain-growth simulation increase dramatically with the number of spatial dimensions. Nevertheless, three-dimensional systems containing in excess of 10^3 grains have been treated successfully using Monte Carlo Potts models [25-29], vertex tracking [30,31], Voronoi tessellation [32], cellular automata [33] and a boundary-tracking approach [34,35].

A prominent method missing from the latter list is the phase-field technique, which, along with Monte Carlo Potts models, arguably represents the most versatile and mature approach for simulating coarsening phenomena, particularly in the presence of multiple phases or gradients of concentration, stress or temperature [23]. In order to understand the difficulty in extending the phase-field model to 3D, it is useful to compare its computational realization to that of the Potts model. In the latter, the simulation cell is composed of a discrete lattice, at the sites of which the values of 'spins' are specified. The phase-field approach, on the other hand, is inherently continuous, in that a set of differential equations are defined at every point in the simulation cell, but the numerical solution of these equations requires discretization, resulting in a set of 'order parameters' being calculated at each site of a discrete lattice spanning the simulation cell. In both models, the boundaries of a grain within the simulation cell are determined by the spatial extent of contiguous lattice sites having identical spin (Potts model) or nearly identical order-parameter (phase-field model) values. Since grain growth is driven by the reduction in free energy associated with a decrease in the total grain-boundary area [2,3], one can simulate coarsening in these models by defining the free energy as an appropriate function of the spin or order-parameter values at the lattice sites. The temporal evolution of the network of boundaries separating the individual grains is then calculated in the Potts model by allowing the spin orientations to change according to a Metropolis algorithm based on Boltzmann statistics [7,36], whereas in the phase-field model the time dependence of the order-parameter values is governed by kinetic equations describing the steepest-descent minimization of the overall free energy [16].

In both the Potts and the phase-field models, the kinetics and topology of coarsening are found to depend on the number of unique grain 'orientations' available to label the individual grains in the simulation cell [7,18,37]. In the case of the Potts model, each discrete spin value corresponds to a distinct grain orientation, and, in the phase-

field approach formulated by Fan and Chen [18,19], each order parameter designates a unique grain orientation. When the number of possible grain orientations is less than the total number of grains in the simulation cell, there is a finite probability for grain growth to occur not by boundary migration but via coalescence, which has never been observed unambiguously in dense polycrystalline specimens [3] (but has received attention of late as a possible growth mechanism for nanometer-sized grains [38,39]). Since, from the standpoint of a Potts or phase-field simulation, the boundaries of an individual grain are defined only by changes in the local grain orientation, coalescence will occur whenever two grains of identical orientation suddenly come into contact, either as the result of a neighbor-switching event (the so-called T1 process [40]) or by annihilation of a nearest-neighbor grain separating the two (the T2 process [40]). Obviously, the smaller the number of distinct grain orientations allowed by the simulation algorithm, the more often coalescence will occur—with potentially dramatic consequences for the grain topology and rate of growth of the average grain size. This was verified by Fan and Chen in their phase-field simulations of coarsening in 2D [18,41]: as the number of order parameters was decreased below 100, the growth rate of the average grain size increased steadily, as did the prevalence of elongated, irregularly shaped grains. Apparently, at least 100 distinct grain orientations are needed to avoid a significant amount of coalescence during a 2-D simulation of grain growth using the Potts or phase-field models.

In the Potts model case, it is a simple matter to increase the number of discrete spin orientations to meet or exceed the initial number of grains in the simulation cell, without increasing the computational overhead [42]; thus, each grain can be assigned a unique orientation, and coalescence can be avoided entirely. In Fan and Chen's phase-field model, however, such a strategy cannot be followed, as both the computational time and the memory requirements increase linearly with the number of order parameters, Q. Indeed, the primary difficulty in extending the phase-field approach to three dimensions lies in the large value of Q needed to obtain grain-growth results untainted by coalescence. This places a severe restriction on the maximum size of the cell that can be handled by a computation of reasonable duration employing an affordable amount of computer memory.

In this paper we describe a modification to Fan and Chen's phase-field model for grain growth that essentially decouples the number of order parameters from the set of conditions determining the computational overhead of the algorithm. The technique takes advantage of an inherent symmetry of the overall free energy with respect to the local exchange of order-parameter values and, by extension, grain orientations. Because the orientations of individual grains can be reassigned without affecting the underlying physics of coarsening, it is possible to avoid the coalescence of neighboring grains by dynamically reassigning orientations such that identical grain orientations never come into contact. In this manner, model-independent results are obtained with Q as small as 20, permitting large-scale simulations of coarsening to be carried out for the first time in 3D using the phase-field approach. In the following section, we describe Fan and Chen's formulation of the phase-field model for grain growth of an ideal polycrystalline specimen and the implementation of grain-orientation reassignment to suppress coalescence. The modified phase-field algorithm is then applied to the problem of ideal grain growth in 3D, the kinetic and topological characteristics of which are summarized and compared to experiment in Section 3. Finally, in Section 4 the phase-field simulation results are compared to those obtained by other methods for simulating three-dimensional coarsening.

2. Phase-field model for grain growth

In the phase-field model developed by Fan and Chen [18,19], the microstructure of a polycrystalline simulation cell is specified by a set of Q continuous order parameters (i.e., field variables) $\{\eta_q(\mathbf{r},t)\}$ $(q = 1,2,\ldots,Q)$ defined at a given time t at each position $\mathbf{r}$ within the simulation cell. The thermodynamics of the simulation algorithm are formulated such that the total free energy is mini-

mized when, within each grain, one and only one field variable takes on a value of 1, and all other order parameters have the value zero. Therefore, the orientation of a given grain can be specified by the index q of the order parameter η_q equal to unity in that grain's interior. Since adjacent grains are distinguished by different q-values, when a grain boundary is crossed the values of two order parameters change continuously from 0 to 1 or vice versa, as illustrated in Fig. 1(a). Because of this continuous variation, grain boundaries in the phase-field model are diffuse, rather than infinitely sharp, as in most other coarsening models [18,43].

Inspired by Allen and Cahn's diffuse-interface theory for antiphase domain boundaries [44], Fan and Chen [18,19] proposed the following expression for the total free energy of a polycrystalline microstructure defined by a set of order parameters $\{\eta_q(\mathbf{r},t)\}$ behaving as described above:

$$F(t) = \int\int\left[f_0(\eta_1(\mathbf{r},t),\eta_2(\mathbf{r},t),\ldots,\eta_Q(\mathbf{r},t)) + \sum_{q=1}^{Q}\frac{\kappa_q}{2}(\nabla\eta_q(\mathbf{r},t))^2\right]d\mathbf{r}, \quad (1)$$

where $\{\kappa_q\}$ are positive constants, and $f_0(\{\eta_q(\mathbf{r},t)\})$ denotes the local free energy density. The latter is defined as

$$f_0(\{\eta_q(\mathbf{r},t)\}) = -\frac{\alpha}{2}\sum_{q=1}^{Q}\eta_q^2(\mathbf{r},t) + \frac{\beta}{4}\Big(\sum_{q=1}^{Q}\eta_q^2(\mathbf{r},t)\Big)^2 + \left(\gamma-\frac{\beta}{2}\right)\sum_{q=1}^{Q}\sum_{s>q}^{Q}\eta_q^2(\mathbf{r},t)\eta_s^2(\mathbf{r},t). \quad (2)$$

In Eq. (2), α, β, and γ are constants; for $\alpha=\beta>0$ and $\gamma>\beta/2$, f_0 has $2Q$ degenerate minima located at $(\eta_1, \eta_2, \ldots \eta_Q)=(\pm1, 0, \ldots, 0), (0, \pm1, \ldots, 0), \ldots,(0, 0, \ldots, \pm1)$. The minima associated with $\eta_q=-1$ can be eliminated as described below, leav-

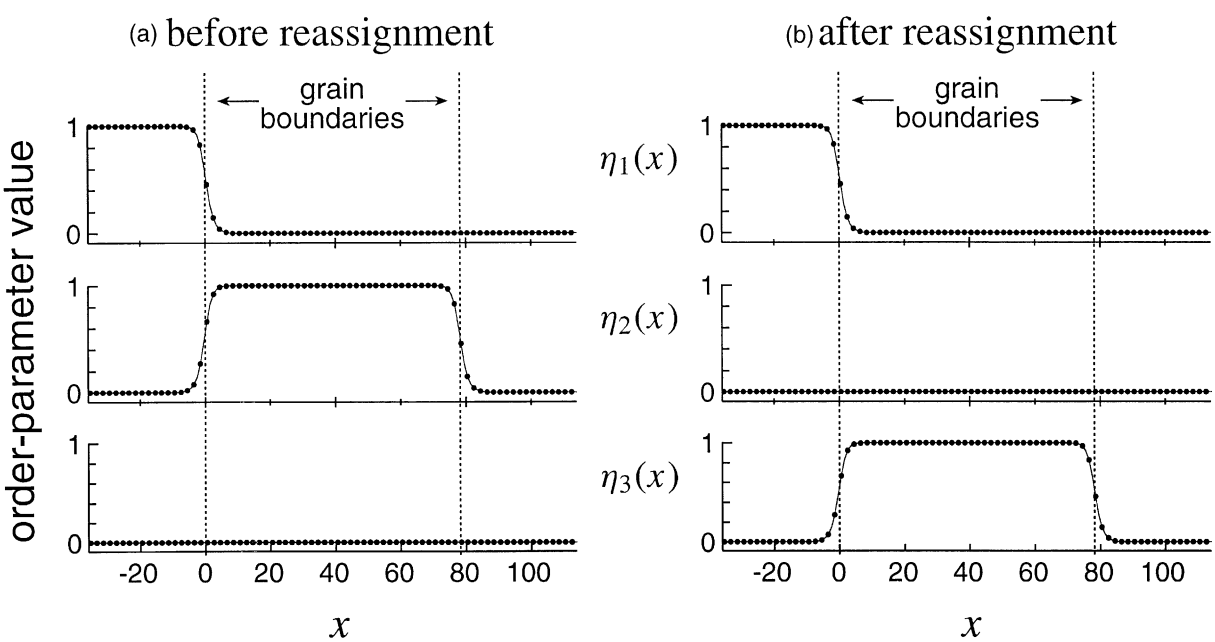

Fig. 1. Section of a one-dimensional simulation grid illustrating the values of the order parameters η_1, η_2 and η_3 as a function of the position x. Grain boundaries are regions of smooth variation in order-parameter values between 0 and 1. In (a), the location of the center grain between $x\approx0$ and $x\approx80$ is specified by η_2. This assignment is changed in (b) by transferring the values of η_2 to η_3 for the corresponding domain in x. Owing to the diffuse nature of grain boundaries in the phase-field model [18,43], values to the left of x=0 and to the right of x=80 must be included in order to retain a smooth gradient following order-parameter reassignment.

ing Q degenerate minima whenever one order parameter takes on the value of unity and the remaining order parameters are zero.

Owing to the dependence of F on the square of the gradient of each field variable, every unit of grain-boundary area (i.e., a location of gradients in η_q) makes a positive contribution to the total free energy of the system. Therefore, there is a thermodynamic driving force for the elimination of grain-boundary area, or, equivalently, for an increase in the average grain size. The reduction in free energy with time t is assumed to follow the trajectory specified by the set of variational derivatives of F with respect to each order parameter, which yield the time-dependent Ginzburg–Landau equations:

$$\frac{\partial \eta_q(\mathbf{r},t)}{\partial t} = -L_q \frac{\delta F(t)}{\delta \eta_q(\mathbf{r},t)} \quad (q = 1,2,\ldots,Q)$$

$$= -L_q\Big(-\alpha\eta_q(\mathbf{r},t) + \beta\eta_q{}^3(\mathbf{r},t) + 2\gamma\eta_q(\mathbf{r},t)\sum_{s\neq q}^{Q}\eta_s{}^2(\mathbf{r},t) - \kappa_q\nabla^2\eta_q(\mathbf{r},t)\Big), \qquad (3)$$

where $\{L_q\}$ are kinetic rate coefficients related to the grain-boundary mobility. As described in the following section, Eq. (3) can be solved numerically at each site of the simulation lattice to obtain the time evolution of the microstructure.

2.1. Discretization and solution of the kinetic equations

After discretizing Eq. (3) in both space and time, we can use the forward Euler equation to evaluate the values of the order parameters over a range of times at the sites $\mathbf{r}$ of a regular lattice spanning the simulation cell:

$$\eta_q(\mathbf{r},t+\Delta t) = \eta_q(\mathbf{r},t) + \frac{\partial \eta_q(\mathbf{r},t)}{\partial t}\Delta t, \quad (q = 1,2,\ldots,Q), \qquad (4)$$

where $\partial\eta_q/\partial t$ is given by Eq. (3). The Laplacian operator of Eq. (3) is discretized as

$$\nabla^2\eta_q(\mathbf{r},t) = \frac{1}{(\Delta x)^2}\sum_{i}^{\text{lnn}}[\eta_q(\mathbf{r}_i,t) - \eta_q(\mathbf{r},t)], \qquad (5)$$

where the index i runs over all first-nearest-neighbor sites $\{\mathbf{r}_i\}$ to site $\mathbf{r}$, and Δx is the uniform spacing between adjacent lattice sites. Periodic boundary conditions are imposed at the edges of the simulation grid. Starting from an initial state $\{\eta_q(\mathbf{r}, 0)\}$, we can combine Eqs. (3), (4) and (5) to solve iteratively for the order-parameter values at integer multiples of the time step Δt.

It is convenient to specify the initial condition—i.e., the starting microstructure—by assigning a small random value $-0.001 < \eta_q(\mathbf{r}, 0) < 0.001$ to each order parameter at each site of the simulation lattice [18,19]. This state corresponds roughly to a supercooled liquid that will crystallize with increasing simulation time until the local free energy density f_0 at most sites assumes a minimum value, with only the sites located at the boundaries between grains making a positive relative contribution to the total free energy. The local minima of f_0 occur whenever a single order parameter takes on a value of either 1 or -1, and, in general, the crystallization process leads to grains corresponding to both possibilities. Therefore, immediately following crystallization the simulation cell contains two distinct types of boundaries: the type illustrated in Fig. 1(a), across which η_j varies from 1 to 0 and $\eta_{k\neq j}$ from 0 to 1, and a second type, in which a single order parameter η_j varies from 1 to -1 or vice versa. The widths of these two boundary types differ slightly, which can lead to a difference in grain-boundary mobility under the discretization conditions applied in this study [45]. Therefore, if we intend to simulate the ideal case of uniform grain-boundary mobilities and energies, we must eliminate one of the boundary types from the simulation cell. This can be accomplished by setting each order parameter equal to its absolute value, effectively restricting the available order-parameter space to that containing only the Q degenerate minima of f_0 involving an order parameter equal to 1. In our simulation runs, the absolute value operation was applied to the $\{\eta_q(\mathbf{r})\}$ values at t=15.0.

Visualization of the simulated microstructure is aided by defining the function

$$\varphi(\mathbf{r},t) = \sum_{q=1}^{Q}\eta_q^2(\mathbf{r},t), \qquad (6)$$

which takes on a value of unity within individual grains and smaller values in the core regions of the boundaries [18,19]. If we map the values of φ to a spectrum of graylevels, then we obtain images like those of Fig. 2(b) and (c), in which the grain boundaries appear as dark regions separating individual grains. The topological properties of the latter—such as number of sides, cross-sectional area, or volume—can be evaluated directly by choosing a threshold value in φ to establish the boundary positions. In this manner, it is possible to quantify the evolution of local and averaged topological grain properties during coarsening.

2.2. Dynamic grain-orientation reassignment

The time evolution of the average grain area $\langle A \rangle$ obtained via the phase-field simulation of two-dimensional coarsening is plotted in Fig. 2(a) for several different values of the number of order parameters, Q. Although the mobility of individual grain boundaries is identical in each simulation run, the rate of growth of $\langle A \rangle$ increases dramatically with decreasing Q. As discussed above, this dependence of the growth rate on Q may be attributed to the increasing rate of grain coalescence as the number of distinct grain orientations (equal to Q) decreases. This explanation is supported by a comparison of the growth-induced microstructures at t=800.0 for Q=10 and Q=100 [Fig. 2(b) and (c)]. The irregularly shaped grains evident in Fig. 2(b) originate when two grains with the same orientation become nearest neighbors, in which case, according to Eq. (3), the gradient in the order parameter corresponding to that orientation is suppressed, and the boundary separating the grains rapidly disappears. The likelihood of coalescence involving a given grain scales with the probability $P(Q)$ that at least one of its second-nearest-neighbor grains shares the same orientation [7]:

$$P(Q) \approx 1 - \left(1 - \frac{1}{Q}\right)^{Z}, \tag{7}$$

where Z denotes the average number of second-nearest-neighbor grains in the microstructure. In the limit of large Q, $P(Q)$ is approximately equal to Z/Q. Since Z=12 for two-dimensional grain growth [37], $P(10)$=0.72 and $P(50)$=0.22. Approximately 110 order parameters are needed to suppress $P(Q)$ below 10%. Thus, it is apparent that coarsening kinetics independent of Q will be obtained only when Q is on the order of 100 or larger.

For a given number of order parameters, the likelihood of coalescence is even higher in three dimensions than in two, as Z is approximately 28 for 3-D polycrystalline microstructures [37]. Thus, more than 200 order parameters would have to be calculated at each grid point in order to simulate

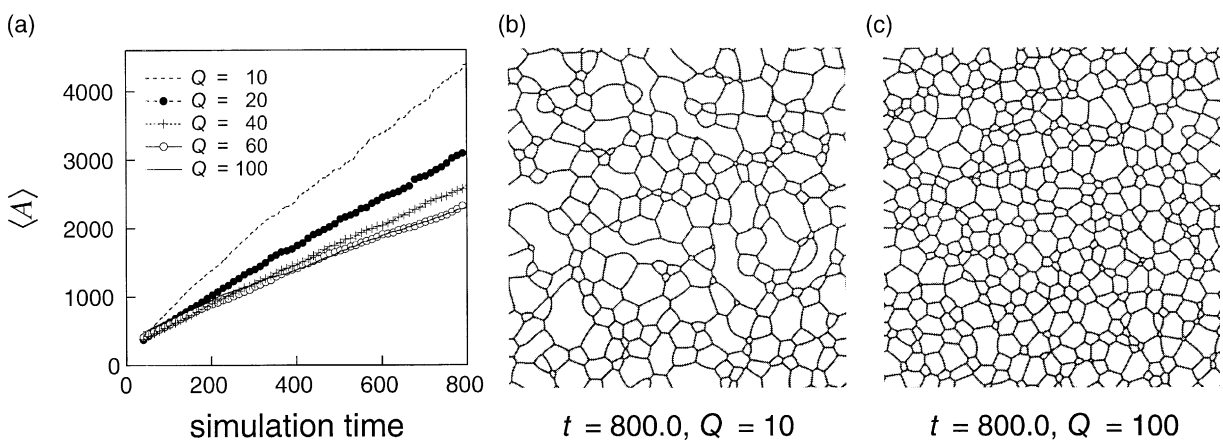

Fig. 2. (a) Evolution of the average grain area $\langle A \rangle$ during phase-field simulations performed on a 512×512 grid with various numbers of order parameters, Q. (b) Microstructure at t=800.0 for Q=10, illustrating the elongated, irregular grain shapes indicative of grain coalescence. (c) Microstructure at t=800.0 for Q=100, manifesting the equiaxed grain topology characteristic of coalescence-free growth.

coalescence-free coarsening in 3D—for a large simulation cell an impractical number both from the standpoint of computing time as well as the amount of memory needed to store so many floating-point values. If the phase-field method is to be useful for simulating three-dimensional grain growth, a way must be found to reduce the rate of coalescence to a negligible level for small values of Q. A potential method for doing so is suggested by the form of Eq. (2), which reveals that the value of f_0 is unaffected by an exchange of order-parameter values at a given site $\mathbf{r}$: i.e., $\eta_q(\mathbf{r},t) \leftrightarrow \eta_s(\mathbf{r},t)$ for $q \neq s$. If such an exchange were carried out for all sites $\{\mathbf{r}\}_q$ associated with a grain of orientation q, then the order-parameter values $\eta_q(\{\mathbf{r}\}_q)$ would be transferred from the η_q order-parameter space to that of η_s [Fig. 1(a) and (b)]. This is equivalent to a reassignment of the grain orientation from q to s. If the domain $\{\mathbf{r}\}_q$ is chosen such that the gradient $\nabla\eta_q$ vanishes at the edges of $\{\mathbf{r}\}_q$, then, according to Eq. (1), the operation will leave the total free energy F unchanged. Hence, it is possible to reassign grain orientations without affecting the thermodynamic driving force for coarsening. An impending coalescence event involving a given grain can be avoided simply by reassigning that grain's orientation to one not associated with any nearby grain.

We have found that a strategy of dynamic grain-orientation reassignment is both easy to implement and effective in suppressing the rate of coalescence. In a two-dimensional simulation cell relatively few distinct grain orientations (i.e., small Q) are necessary to establish a grain-orientation mapping in which no grain shares the same orientation with its first or second-nearest neighbors. This can be accomplished by maintaining a list of the order-parameter indices of the nearest and next-nearest grains to each grain present in the simulation cell. At a particular time step, each grain is checked for a match between its orientation and those in the list: if a match is found, the order-parameter values corresponding to the orientation of the given grain are reassigned to a new order parameter not present in the list. The orientation of each grain in the simulation cell is examined and (if necessary) reassigned sequentially until all first or second-nearest-neighbor orientation matches have been eliminated. Experience shows that, for a 2-D simulation cell, such a simple procedure converges rapidly to a match-free grain-orientation mapping for Q as small as 17. The iterative evaluation of Eq. (4) can then be advanced for several time steps until one or more grains have been eliminated from the simulation cell, at which point the grain-orientation mapping must be updated to account for the new topological relationship between grains. The computational overhead associated with the reassignment of grain orientations is comparable to that of a single iteration of Eq. (4). Consequently, the much smaller value of Q made possible by the orientation-reassignment procedure results in a dramatic savings in overall computational time for a coalescence-free simulation.

In three dimensions, the average number of first and second-nearest-neighbor grains is more than twice as large as in two dimensions [37]; hence, approximately 50 order parameters would be needed to implement the above scheme in 3D. Alternatively, one can make do with a smaller Q if one ignores the second-nearest-neighbor grains and focuses exclusively on eliminating matches in grain orientation between first-nearest-neighbor grains. In the event that two grains of identical orientation come into contact, it is necessary to reassign the orientation of one of the grains immediately; otherwise, owing to the rapidity with which the boundary between such grains is eliminated by Eq. (3), there will be no opportunity to avoid a coalescence event by grain-orientation reassignment at a later time. As in 2D, the computational time needed to inspect the microstructural topology for incipient nearest-neighbor orientation matches is comparable to a single iteration of the routine used to solve the partial differential equations governing the evolution of the order parameters. Because a Q of 20 is more than sufficient to establish a grain-orientation mapping free of first-nearest-neighbor matches in 3D, the reduction in the number of order parameters made possible by the orientation-reassignment scheme more than makes up for the extra time associated with a check for impending coalescence events after each iteration of Eq. (4). Indeed, only the concomitant reduction in storage and computational time renders the large-scale coalescence-free simulation of

grain growth tractable in 3D using Fan and Chen's formulation of the phase-field approach. Fig. 3 illustrates the similarity in growth rates obtained by a 3-D phase-field simulation performed using the standard algorithm with Q=100 and one employing dynamic grain-orientation reassignment with Q=20.

3. Three-dimensional grain growth in the phase-field model

In order to study the statistically averaged kinetics and topological features of ideal three-dimensional grain growth in the phase-field model, computer simulations were performed on a simple-cubic lattice with 180×180×180 grid points, Q=20 order parameters and dynamic grain-orientation reassignment performed after each time step. As in the 2-D phase-field simulations of Fan et al. [18,19], the coefficients appearing in Eq. (3) were chosen to have the values $\alpha=\beta=\gamma=1$, $\{\kappa_q\}=2$ and $\{L_q\}=1$ for q=1 to Q. The lattice step size Δx was set to 2.0, and a time step Δt of 0.1 was employed in all simulations. As illustrated in the sequence of images in Fig. 4, the initial supercooled liquid state (described by random order-parameter values $\{|\eta_q|\} < 0.001$ crystallizes fully within the first 300 time steps to a dense packing of nearly 6000 grains. With increasing simulation time, grains are eliminated via boundary migration and, owing to the conservation of total volume, the average grain size increases steadily. Following 8000 time steps, less than 4% of the initial grain population remains in the simulation cell. Because the cell must fully crystallize before grain orientations can be reassigned dynamically, some coalescence of grains of like orientation occurs in the time interval $t<30.0$, leading to the telltale presence of elongated, irregular grains. The grain-orientation reassignment algorithm was turned on at t=30.0, at which time coalescence stops and the elongated grains begin to take on more equiaxed shapes. The latter process is complete by $t\approx150$, from which point on the microstructure should be characteristic of coalescence-free growth. In order to reduce the amplitude of statistical fluctuations in the values for the kinetic and topological parameters extracted from the simulation data, we combined the results of three simulations of 8000 time steps starting from different initial liquid states (specified by distinct seed values for the random-number generator used to assign the initial order-parameter values).

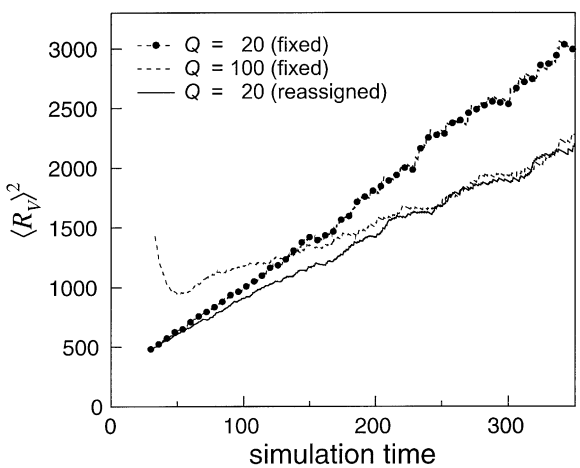

Fig. 3. Time evolution of the square of the average grain size $\langle R_V\rangle$ (determined as in Sec. 3.1) in phase-field simulations of grain growth performed on a 110×110×110 grid. Following an initial transient, a simulation with Q=20 order parameters and dynamic grain-orientation reassignment yields a growth rate that is indistinguishable from that of a Q=100 simulation with fixed grain orientations. (The initial offset between the two curves arises from the occurrence of crystallite nucleation in the Q=100 simulation over a longer time than in the Q=20 simulation. Incomplete crystallization of the simulation cell is the origin of the (apparent) negative growth in the Q=100 simulation at $t<50$.) In the absence of orientation reassignment, reducing Q from 100 to 20 results in a much faster increase in $\langle R_V\rangle^2$, indicating significant grain growth through coalescence.

3.1. Grain-growth kinetics

According to analytic theories for normal grain growth [2,3], following an initial transient of duration t_0, the average grain size $\langle R\rangle$ is expected to increase with time t as $\langle R\rangle^2(t) = \langle R\rangle^2(t_0) + k(t-t_0)$, where $\langle R\rangle(t_0)$ denotes the average grain size at t_0, and k is a constant related to the grain-boundary mobility. The size of a grain in the simulation cell is determined by counting the lattice points located within the boundaries of the grain,[1] multiplying by

[1] Before determining the individual grain volumes, all lattice points located within the the grain-boundary regions—defined

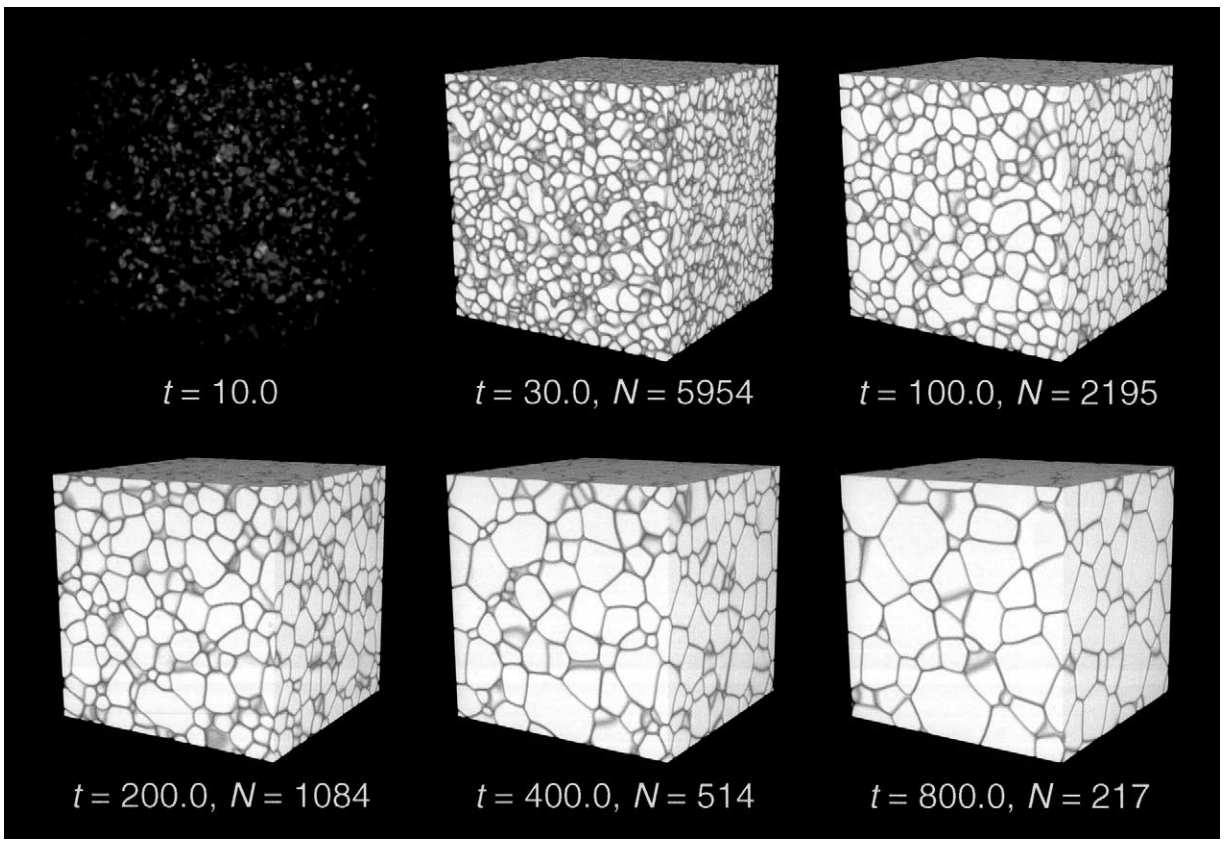

Fig. 4. Phase-field simulation of microstructural evolution performed on a 180×180×180 simple-cubic grid, visualized by mapping the values of the function $\varphi(\mathbf{r})$ [Eq. (6)] to a spectrum of graylevels. The elapsed time t and the number of grains N are specified under each image. The microstructure at t=10.0 illustrates the homogeneous nucleation of crystallites from the supercooled liquid initial state.

$(\Delta x)^3$ to obtain the grain volume V, and then defining R_V to be the *diameter* of a sphere of equivalent volume: $R_V \equiv (6V/\pi)^{1/3}$. Averaging over all of the grains present in the cell (and over the three separate simulation runs), we obtain the time evolution of $\langle R_V \rangle$ plotted in Fig. 5. Using the equation

$$\langle R_V \rangle^m(t) = \langle R_V \rangle^m(t_0) + k(t - t_0) \quad (8)$$

with refinable parameters m, $\langle R_V \rangle(t_0)$ and k, we perform a weighted nonlinear least-squares fit to the data of Fig. 5 for $t \geq t_0$=150.0 and obtain a value for the growth exponent m of 2.02±0.02, which agrees with the theoretical prediction, with experiments performed on single-phase polycrystalline samples at temperatures close to the melting point [3] and with computer simulations carried out in 2D [6,10,18,46,47] as well as in 3D [25–32,34].

3.2. Distribution of grain sizes

In Fig. 6(a) the distribution $f(R_V, t)$ of grain sizes is plotted at several simulation times as a function of the normalized grain size $R_V/\langle R_V \rangle$. At times $t \lesssim 100$, the shape of the distribution evolves continuously, with the maximum shifting to larger sizes and the width increasing slightly. At later times, the form of the grain-size distribution is

by $\varphi(\mathbf{r},t) < 0.8$—are assigned to the nearest grain. Consequently, each grain boundary is divided equally among two grain volumes, and the total volume of the grains is always equal to the overall volume of the simulation cell.

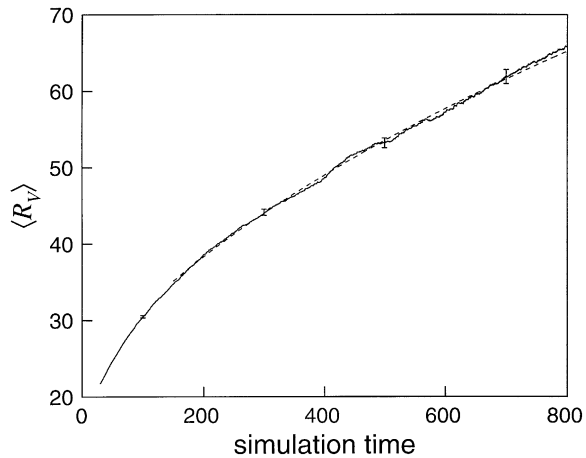

Fig. 5. Time evolution of the average grain size $\langle R_V \rangle$ in phase-field simulations of grain growth performed on a 180×180×180 grid (solid curve). Dashed curve is the result of a nonlinear least-squares fit of Eq. (8) over the time interval $150.0 \leq t \leq 800.0$, weighted by the statistical uncertainties indicated by the vertical bars.

essentially stationary, which is indicative of the scaling behavior commonly observed in experimental studies of normal grain growth and in simulations of coarsening performed in 2D and in 3D [2,3,6,48]. The true shape of the steady-state distribution induced by grain growth, $\hat{f}(R_V/\langle R_V \rangle)$ has been the subject of lively discussion ever since Hillert [49] derived a mean-field theory consistent with a parabolic growth law for $\langle R \rangle(t)$ [i.e., $m=2$ in Eq. (8)] and scaling behavior for $f(R,t)$, primarily because the sharply peaked and rather-skewed form of $\hat{f}(R/\langle R \rangle)$ predicted by the Hillert theory deviates significantly from the roughly lognormal shape usually found in experiment [50–52]. In Fig. 6(b) the Hillert distribution is compared to the distribution of grain sizes measured in a steel sample [53] and to the steady-state distribution inferred from our phase-field simulations by averaging over the distributions present at $t=200.0$, 400.0 and 800.0 in the simulation cell. Clearly, the Hillert distribution is a poor approximation to the experimental data, and the simulation results represent only a partial improvement in this regard, as the steady-state grain-size distribution of the simulated microstructures is more symmetric and broader than the lognormal distribution of the steel sample. This discrepancy between simulation and experiment might be attributed to the influence of impurity atoms, which are always present to a certain extent in the grain boundaries of real materials, or perhaps to the unphysical assumption of uniform grain-boundary mobilities and energies that underlies the simulation algorithm. Studies attempting to incorporate impurity effects or a realistic spectrum

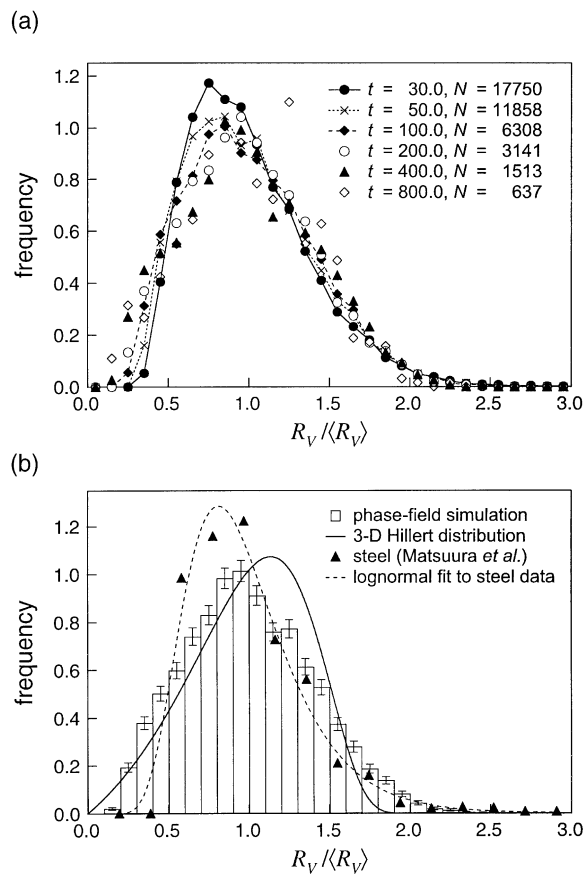

Fig. 6. (a) Distribution of grain sizes in phase-field simulations of grain growth performed on a 180×180×180 grid, plotted as a function of the normalized grain size $R_V/\langle R_V \rangle$ for several simulation times t. The quantity N specifies the number of grains in the simulation cell (obtained by combining the results of three separate simulation runs at the indicated times). (b) Steady-state grain-size distribution (histogram) found by 3-D phase-field simulation, calculated as a weighted average over the distributions in the scaling regime at $t=200.0$, 400.0 and 800.0. For comparison, the steady-state distribution predicted by the Hillert theory [49] is plotted as the solid curve along with experimental data obtained on SUS304 stainless steel by Matsuura et al. [53]. The dashed curve is a fit of a lognormal function to the data points for steel.

of grain-boundary mobilities and energies in computer simulations of grain growth have begun to appear in the literature [27,37,54–63], but a consensus regarding the origin of the non-lognormal shape of the simulated grain-size distributions has yet to emerge.

3.3. Topology of grain-growth-induced microstructures

As emphasized in the pioneering work of Smith [64,65], grain growth involves the complex interplay of competing topological requirements: on the one hand, the establishment of local equilibrium in the network of grain boundaries (i.e., force balance at triple junctions and quadruple points of the interface tensions arising from the excess energy of the grain boundaries) and, on the other, the maintenance of a space-filling ensemble of grains. The topological aspects of coarsening can be quantified by evaluating statistical averages and distributions of various parameters characterizing the shapes of the individual grains in the growth-induced microstructure. Primary examples of such fundamental topological parameters are the number of faces (sides) per grain, F, and its distribution $g(F,t)$. Adopting the convention that F is evaluated for a given grain as if that grain were isolated from its neighbors (in other words, each face contributes to the F of two different grains), we find in our simulations that, at times $t \gtrsim 150$, the average number of faces per grain, $\langle F \rangle$, takes on a constant value of 13.7±0.1, and the distribution of F assumes the steady-state shape plotted in Fig. 7. In Table 1, this value for $\langle F \rangle$ is compared to experimental measurements of the same quantity performed on a variety of polycrystalline microstructures; furthermore, the table includes the corresponding values for a space-filling ensemble of Kelvin or Williams tetrakaidecahedra [25] and for the Poisson–Voronoi tessellation [66], which is frequently used to model polycrystalline microstructures. A similar comparison can be carried out with the average number of edges per grain, $\langle E \rangle$, and the average number of vertices (corners) per grain, $\langle V \rangle$, which take on the values 34.8±0.2 and 23.1±0.2, respectively, in the microstructures generated in the steady-state regime of the phase-field simulations. A final topological parameter describing the grain shape, the distribution of the number of edges per grain face, E_F, is plotted in Fig. 8 for the scaling regime ($t \gtrsim 150$) of the phase-field simulations. The average value $\langle E_F \rangle = 5.07 \pm 0.01$ is comparable to that of several polycrystalline systems studied experimentally (Table 1), and reasonably good agreement is found between the E_F-distribution generated by phase-field simulation and that measured in an Al–Sn alloy using stereoscopic microradiography [67]. In general, the topological parameters of the microstructures generated by 3-D phase-field simulation are closer to those obtained from real materials than to those of an ensemble of space-filling tetrakaidecahedra or those of the Poisson–Voronoi tessellation. This suggests that the grain-growth simulation algorithm yields a more realistic model of the network of grain boundaries in a polycrystalline solid—a fact that should be relevant to any computational effort to determine the influence of microstructure on the properties of a polycrystalline sample.

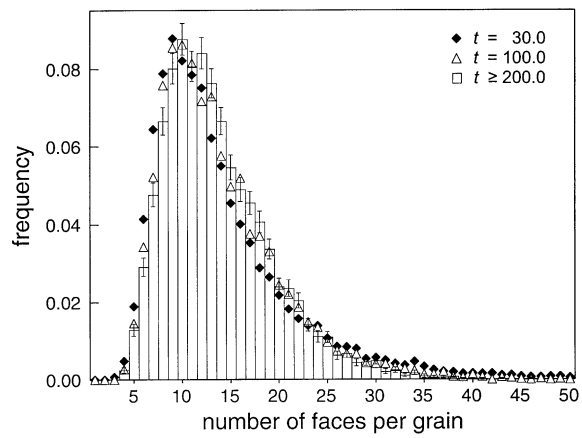

Fig. 7. Distribution of the number of faces (sides) per grain obtained in phase-field simulations of grain growth performed on a 180×180×180 grid. The distribution takes on a stationary form for simulation times $t \gtrsim 150$; the steady-state distribution (histogram) was computed from a weighted average of the face-number distributions at t=200.0, 400.0 and 800.0.

For a single simply connected polyhedron, the quantities F, E and V satisfy Euler's equation [64], $F-E+V=2$. Since this relation applies equally well to each of the cells of a 3-D polycrystalline microstructure, we have

Table 1
Topological parameters of 3-D microstructures generated by phase-field simulation, measured in a variety of cellular materials, or modeled as a space-filling ensemble of tetrakaidecahedra or as a Poisson–Voronoi tessellation. The quantity $\langle E_F \rangle$ designates the average number of edges per grain face, whereas $\langle F \rangle$, $\langle E \rangle$ and $\langle V \rangle$ denote the respective average number of faces (sides), edges and vertices per grain (evaluated as if each grain were an isolated polyhedron)

Sample	$\langle E_F \rangle$	$\langle F \rangle$	$\langle E \rangle$	$\langle V \rangle$	Ref.
Phase-field simulation	5.07	13.7	34.8	23.1	
Al–Sn	5.06	12.48	31.52	21.04	[65,67]
β-brass	5.14	14.5	37.35	24.85	[25,69]
β-brass	4.92	11.16	27.48[a]	18.32[a]	[70]
Fe	5.11	13.42	34.26[a]	22.84[a]	[71]
Austinitic steel	5.07–5.10[b]	12.58–13.38[b]	31.73–34.13[b]	21.15–22.76[b]	[71,72]
SUS304 steel	4.4	14	31	19	[53]
Foam	5.11	13.4	34.2[a]	22.8[a]	[73]
Tetrakaidecahedra	5.143	14	36	24	[25]
Poisson–Voronoi	5.228	15.535	40.606	27.071	[66,74]

[a] Calculated from $\langle F \rangle$ using Eq. (11a,b).
[b] Topological parameters increased monotonically as a function of annealing time at 1050°C; tabulated values correspond to annealing times of 30 sec and 50 min [71,72].

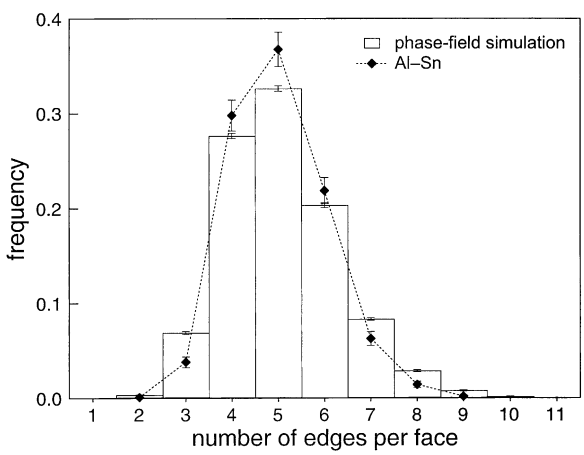

Fig. 8. Distribution of the number of edges per grain face (side) in the scaling regime ($t \gtrsim 150$) of phase-field simulations of grain growth performed on a 180×180×180 grid. The corresponding distribution measured by Williams and Smith [67] in polycrystalline Al doped with Sn (segregated to the grain boundaries) is plotted for the sake of comparison.

$$\langle F \rangle - \langle E \rangle + \langle V \rangle = 2 \tag{9}$$

for any space-filling ensemble of cells, provided the quantities F, E and V are evaluated as if the individual cells were isolated polyhedra. Considerations of topological stability in 3D (i.e., invariance of the topological properties of the microstructure under small deformation) dictate that exactly four edges meet at each vertex of a cellular solid [40,68]. Hence, on the surface of each grain in a topologically stable polycrystal, three edges meet at any vertex. Since each edge connects two vertices, the relation $3V=2E$ must hold for each grain, and, averaging over all of the grains in the sample, we must obtain

$$3\langle V \rangle = 2\langle E \rangle. \tag{10}$$

Combining Eqs. (9) and (10), we can express any two average grain-shape parameters in terms of the third [64]; for example,

$$\langle E \rangle = 3\langle F \rangle - 6. \tag{11a}$$

$$\langle V \rangle = 2\langle F \rangle - 4. \tag{11b}$$

Furthermore, under the same assumption of topological stability, one can derive the relation

$$\langle E_F \rangle = 6 - \frac{12}{\langle F \rangle} \tag{12}$$

between the average number of edges per face, $\langle E_F \rangle$, and the average number of faces per grain, $\langle F \rangle$ [64]. The extent to which Eq. (10)—and, by extension, Eqs. (11) and (12)—is satisfied by the average topological parameters of a given polycrystalline microstructure is indicative of the

degree to which the corresponding network of grain boundaries fulfills the condition for topological stability in 3D. As the entries in Table 1 indicate, the microstructures generated during the 3-D phase-field simulations satisfy Eqs. (10), (11a,b) and (12) closely at simulation times $t \gtrsim 150$, indicating that topological stability is achieved and maintained throughout the scaling regime of each simulation run.

4. Three-dimensional grain growth in various simulation models

Prior to our studies employing the phase-field approach, large-scale computer simulations of ideal grain growth were carried out in 3D using the Monte Carlo Potts model [25–29], a boundary-tracking method [34,35] and the vertex method [30,31]. Many aspects of the results of each of these investigations lie in quantitative agreement with one another and with our phase-field results. For example, as mentioned in Section 3.1, all of the simulation models yield a value of 2 for the grain-growth exponent m of Eq. (8), and they find that the grain-size distribution $\hat{f}(R_V/\langle R_V\rangle)$ takes on a steady-state shape following an initial transient in the evolution of the microstructure. Further similarities are evident in the values for the topological parameters $\langle E_F\rangle$, $\langle F\rangle$, $\langle E\rangle$ and $\langle V\rangle$ of the simulation-generated microstructures in the scaling regime (Table 2). In most cases, the differences between the topological averages calculated in each model lie within the bounds of statistical uncertainty determined by the finite number of grains present in a given simulation cell.

Nevertheless, examining the distributions—rather than the average values—of R_V and the topological parameters, one finds evidence for discrepancies between the various simulation results. In Fig. 9(a) the shape of $\hat{f}(R_V/\langle R_V\rangle)$ obtained by the phase-field method is compared to that of four different simulations based on the Monte Carlo Potts model. Only the distribution calculated by Miyake [28] agrees with the phase-field result in both the location of the frequency maximum as well as in the rate at which the distribution falls off at larger grain sizes [76]. The more asymmetric, approximately lognormal shape of the distribution calculated by Anderson et al. [25] can be traced to the fact that only Q=48 spin values were used to label distinct grain orientations in their simulations, resulting in a non-negligible rate of grain coalescence and an increased population of large grains. The distribution found by Saito [27] is significantly narrower than that found by the other methods, and, most strikingly, it falls off to zero much faster at large R_V. The origin of this behavior is unclear. Song et al. [29,71,77] reported that a true stationary state of $\hat{f}(R_V/\langle R_V\rangle)$ was not reached in their simulations, with the peak of the distribution shifting slowly to larger R_V with increasing simulation time. The grain-size distribution present at the longest time of 1100 Monte Carlo steps [plotted in Fig. 9(a)] appears to be somewhat broader than the others, which may again be related to the occurrence of grain coalescence. Of the four Monte Carlo simulations included in Fig. 9(a), it appears that only Miyake's simulation [28] suppresses both the occurrence of grain coalescence (by assigning a unique spin value to each grain in the starting configuration) and the influence of lattice anisotropy (by performing the simulations at a high effective temperature [36,78]). These facts, coupled with the large grid size of 300×300×300, suggest that Miyake's steady-state distribution is least distorted by intrinsic limitations of the underlying Monte Carlo Potts model.

The steady-state grain-size distributions found by two other 3-D grain-growth simulation methods are plotted in Fig. 9(b). The distribution obtained by Wakai et al. [34] using a 3-D implementation of the Surface Evolver program [79] is nearly identical to the phase-field result and to that found by Miyake using the Monte Carlo approach. Only at large R_V near $2\langle R_V\rangle$ does the former fall of more rapidly than the latter two distributions, although the range of grain sizes over which the deviation appears is rather narrow. The same behavior is manifested by the steady-state distribution obtained by Weygand et al. [31] using the vertex method. Their distribution also appears to be peaked at a slightly larger value of $R_V/\langle R_V\rangle$ than the others, and the distribution has a finite value at $R_V \rightarrow 0$. The overall deviation between the four distributions plotted in Fig. 9(b), however, is so small that simu-

Table 2
Topological parameters of polycrystalline microstructures in the scaling regime, as generated by various algorithms for simulating three-dimensional ideal grain growth. The quantity $\langle E_F \rangle$ designates the average number of edges per grain face, whereas $\langle F \rangle$, $\langle E \rangle$ and $\langle V \rangle$ denote the respective average number of faces (sides), edges and vertices per grain

Simulation	$\langle E_F \rangle$	$\langle F \rangle$	$\langle E \rangle$	$\langle V \rangle$	Ref.
Phase-field	5.07	13.7	34.8	23.1	
Monte Carlo	5.14	12.85	33.04	22.19	[25]
Monte Carlo	–	13.7	–	–	[75]
Monte Carlo	–	15.3[a]	–	–	[27]
Monte Carlo	5.05	13.3[b]	34.2[b]	22.8[b]	[71]
Surface Evolver	5.05[c]	13.5	34.1	22.6	[34,35]
Vertex	5.01	13.8	–	–	[31]

[a] Value calculated from the faces-per-grain distribution shown in Fig. 9 of Ref. [27].
[b] In this study, the topological parameters $\langle F \rangle$, $\langle E \rangle$ and $\langle V \rangle$ did not reach steady state; the values tabulated correspond to the late stage of the simulation at ~1100 Monte Carlo steps.
[c] Value calculated from the edges-per-face distribution shown in Fig. 16 of Ref. [34].

lations would have to be performed on a much larger scale (i.e., with many more grains) in order to verify the existence of statistically significant discrepancies.

The similarity of the grain-growth-induced microstructures generated by the phase-field, Surface Evolver and vertex methods is underlined by the data of Figs. 10 and 11, in which the respective distributions of the number of faces per grain and edges per face are plotted. No such data were reported for the Monte Carlo simulations carried out by Miyake; therefore, the results of other studies employing the Monte Carlo Potts model are included in Figs. 10 and 11. In the case of the number of faces per grain, the distributions found by the Monte Carlo approach deviate significantly from those of the other methods—a fact that is also reflected in the values for $\langle F \rangle$ obtained by averaging over the distributions of Fig. 10 (Table 2). The same is true of the distributions of E_F, although in this case the phase-field result is roughly intermediate between the more asymmetric Monte Carlo distribution and the more sharply peaked finding of the Surface Evolver and vertex methods. Values for $\langle E_F \rangle$, on the other hand, were nearly identical in all cases.

Echoing the case in 2D, the kinetic and topological aspects of ideal 3-D grain growth as calculated by a variety of simulation methods are qualitatively indistinguishable and quantitatively similar, provided the occurrence of grain coalescence is suppressed. The choice of an algorithm for simulating coarsening phenomena can therefore be made in consideration of the ease with which it can be adapted to the problem at hand. For example, the vertex method is ideally suited to studies involving drag forces acting on the triple junctions of the grain-boundary network [80,81], while the phase-field approach is a natural choice for situations involving microstructures coupled to concentration or stress gradients in the bulk [1,82,83]. One must bear in mind, however, that none of the currently available simulation methods generates microstructural results agreeing completely with experiment—as demonstrated in particular by the shape of the grain-size distribution in the scaling regime. In real polycrystalline solids, the grain-boundary mobilities and energies depend on the misorientation of neighboring crystallites as well as on the segregation of impurities to the grain-boundary cores [3,4]. The generalization of 3-D grain-growth simulation methods to include misorientation-dependent properties and impurity effects may hold the greatest promise for resolving the remaining discrepancies between simulation and experiment [84,85].

5. Conclusions

The implementation of dynamic grain-orientation reassignment in Fan and Chen's formulation

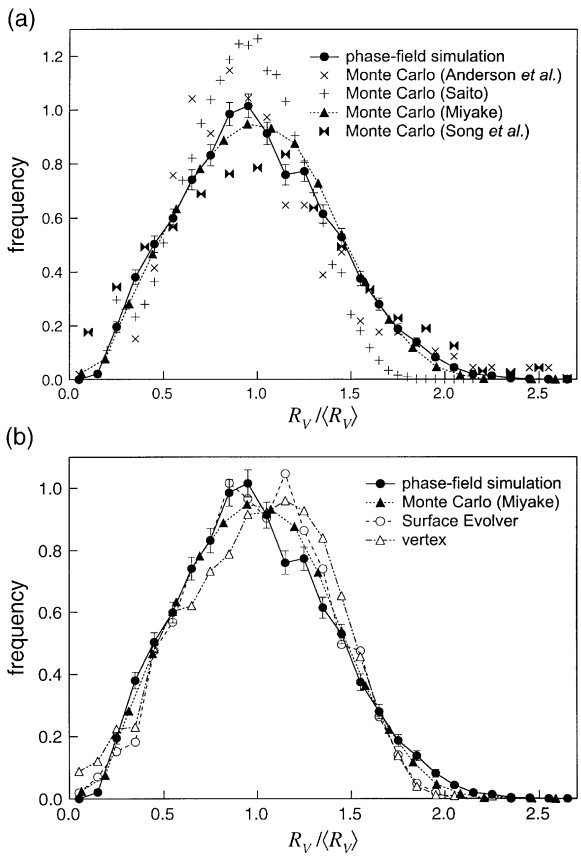

Fig. 9. Steady-state grain-size distributions generated by various algorithms for simulating three-dimensional grain growth. (a) The result of phase-field simulations [Fig. 6(b)] compared to the distributions obtained by the Monte Carlo Potts models of Anderson et al. [25], Saito [27], Miyake [28,76] and Song et al. [29,71,77]. (b) Comparison of the phase-field result to that of the Monte Carlo method of Miyake, the Surface Evolver approach of Wakai et al. [34] and the vertex method of Weygand et al. [31].

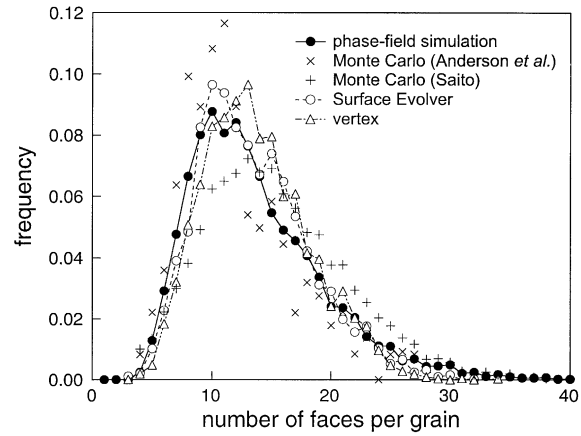

Fig. 10. Comparison of the distributions of the number of faces (sides) per grain in the scaling regime obtained by phase-field simulation (Fig. 7), the Monte Carlo Potts models of Anderson et al. [25] and Saito [27], the Surface Evolver approach [34] and the vertex method [31].

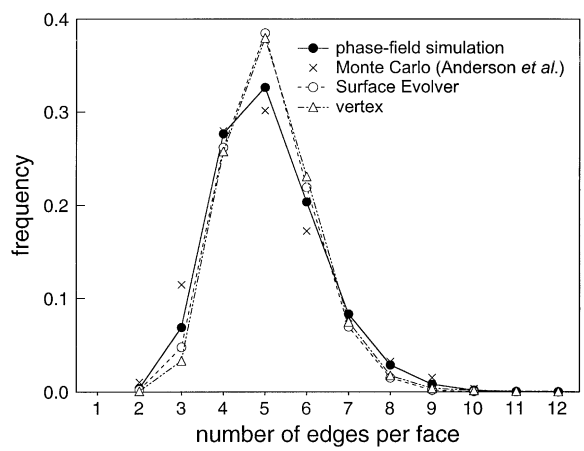

Fig. 11. Comparison of the distributions of the number of edges per grain face in the scaling regime obtained by phase-field simulation (Fig. 8), the Monte Carlo Potts model of Anderson et al. [25], the Surface Evolver approach [34] and the vertex method [31].

of the phase-field model for grain growth allows this method to be extended to the large-scale simulation of coarsening in 3D. The reassignment of grain orientations avoids the occurrence of grain growth through coalescence, and it greatly reduces the computational overhead of the phase-field algorithm by restricting the necessary number of order parameters to $Q \approx 20$. Consequently, coalescence-free simulation of the coarsening of thousands of grains becomes tractable, from which reliable statistical averages of kinetic and topological parameters can be extracted. The evolution of the average grain size of an ideal polycrystal with uniform grain-boundary mobilities and energies is found to follow a parabolic growth law, and the distributions of gram sizes and topological parameters describing the grain shape take on invariant forms at simulation times beyond an initial transient. Detailed comparison with the results of other methods for simulating grain growth in 3D find

close agreement of both kinetic and topological microstructural parameters, provided growth through coalescence is completely suppressed during the simulation. Discrepancies remain, however, between experimental investigations of grain growth and the results of simulation, particularly with respect to the shape of the grain-size distribution in the scaling regime. The incorporation of a spectrum of grain-boundary mobilities and energies as well as impurity effects into the simulation algorithms may help to resolve this inconsistency.

Acknowledgements

The authors are grateful to V. Tikare for providing the computer code that served as the basis for subroutines used to evaluate the topological properties of the simulated microstructures. Financial support was provided by the Deutsche Forschungsgemeinschaft [SFB 277 and Habilitation fellowship (CEK)], the University of the Saarland and the US National Science Foundation (DMR-0122638).

References

[1] Raabe D. Computational materials science: the simulation of materials microstructures and properties. Weinheim, Germany: Wiley-VCH; 1998.
[2] Atkinson HV. Acta metall 1988;36:469.
[3] Humphreys FJ, Hatherly M. Recrystallization and related annealing phenomena. Oxford: Pergamon Press. 1996. Chapter 9.
[4] Gottstein G, Shvindlerman LS. Grain boundary migration in metals: thermodynamics, kinetics, applications. Boca Raton, FL: CRC Press, 1999.
[5] Frost HJ, Thompson CV. Curr Op Solid State Mater Sci 1996;1:361.
[6] Thompson CV. Solid State Phys 2001;55:269.
[7] Anderson MP, Srolovitz DJ, Crest GS, Sahni PS. Acta metall 1984;32:783.
[8] Srolovitz DJ, Anderson MP, Sahni PS, Crest GS. Acta metall 1984;32:793.
[9] Kawasaki K, Nagai T, Nakashima K. Phil Mag B 1989;60:399.
[10] Weygand D, Bréchet Y, Lépinoux J. Phil Mag B 1998;78:329.
[11] Frost HJ, Thompson CV, Howe CL, Whang J. Scripta metal mater 1988;22:65.
[12] Marthinsen K, Hunderi O, Ryum N. In: Chen L-Q, Fultz B, Cahn JW, Manning JR, Morral JE, Simmons JA, editors. Mathematics of Microstructural Evolution. Warrendale, PA: The Minerals, Metals & Materials Society; 1996. p. 15–22.
[13] Telley H, Liebling TM, Mocellin A. Phil Mag B 1996;73:395.
[14] Telley H, Liebling TM, Mocellin A. Phil Mag B 1996;73:409.
[15] Geiger J, Roósz A, Barkóczy P. Acta mater 2001;49:623.
[16] Chen L-Q, Yang W. Phys Rev B 1994;50:15752.
[17] Steinbach I, Pezzolla F, Nestler B, Seeßelberg M, Prieler R, Schmitz GJ. Physica D 1996;94:135.
[18] Fan D, Chen LQ. Acta mater 1997;45:611.
[19] Fan D, Geng C, Chen L-Q. Acta mater 1997;45:1115.
[20] Lusk MT. Proc R Soc London A 1999;455:677.
[21] Kobayashi R, Warren JA, Carter WC. Physica D 2000;140:141.
[22] Lobkovsky AE, Warren JA. J Crystal Growth 2001;225:282.
[23] Tikare V, Helm EA, Fan D, Chen LQ. Acta mater 1999;47:363.
[24] Maurice C. In: Gottstein G, Molodov D, editors. Recrystallization and Grain Growth, Vol. 1. Berlin: Springer-Verlag; 2001. pp. 123–34.
[25] Anderson MP, Grest GS, Srolovitz DJ. Phil Mag B 1989;59:293.
[26] Glazier JA. Phys Rev Lett 1993;70:2170.
[27] Saito Y. ISIJ Intern 1998;38:559.
[28] Miyake A. Contrib Mineral Petrol 1998;130:121.
[29] Song X, Liu GJ. Univ Sci Tech Beijing 1998;5:129.
[30] Fuchizaki K, Kusaba T, Kawasaki K. Phil Mag B 1995;71:333.
[31] Weygand D, Bréchet Y, Lépinoux J, Gust W. Phil Mag B 1999;79:703.
[32] Xue X, Righetti F, Telley H, Liebling TM. Phil Mag B 1997;75:567.
[33] Raabe DI. In: Weiland H, Adams BL, Rollett AD, editors. Grain Growth in Polycrystalline Materials III. Warrendale, PA: The Minerals, Metals & Materials Society; 1998. p. 179–85.
[34] Wakai F, Enomoto N, Ogawa H. Acta mater 2000;48:1297.
[35] Wakai F. J. Mater Res 2001;16:2136.
[36] Holm EA, Battaile CC. JOM 2001;53(9):20.
[37] Radhakrishnan B, Zacharia T. Metall Mater Trans A 1995;26A:167.
[38] Harris KE, Singh VV, King AH. Acta mater 1998;46:2623.
[39] Moldovan D, Wolf D, Phillpot SR. Acta mater 2001;49:3521.
[40] Stavans J. Rep Prog Phys 1993;56:733.
[41] Chen LQ, Fan DN, Tikare VI. In: Weiland H, Adams BL, Rollett AD, editors. Grain Growth in Polycrystalline Materials III. Warrendale, PA: The Minerals, Metals & Materials Society; 1998. p. 137–46.
[42] Hassold GN, Holm EA. Comput Phys 1993;7:97.
[43] Fan D, Chen L-Q. Phil Mag Lett 1997;75:187.

[44] Allen SM, Cahn JW. Acta metall 1979;27:1085.
[45] Fan D, Chen L-Q, Chen SP. Mater Sci Eng A 1997;A238:78.
[46] Grest GS, Anderson MP, Srolovitz DJ. Phys Rev B 1988;38:4752.
[47] Marthinsen K, Hunderi O, Ryum N. Acta mater 1996;44:1681.
[48] Hu H. Can Metall Q 1974;13:275.
[49] Hillert M. Acta metall 1965;13:227.
[50] Okazaki K, Conrad H. Trans JIM 1972;13:198.
[51] Rhines FN, Patterson BR. Metall Trans A 1982;13A:985.
[52] Pande CS. Acta metall 1987;35:2671.
[53] Matsuura K, Itoh Y, Ohmi T, Ishii K. Mater Trans JIM 1994;35:247.
[54] Mehnert K, Klimanek P. Comput Mater Sci 1996;7:103.
[55] Mehnert K, Klimanek P. Comput Mater Sci 1997;9:261.
[56] Gao J, Thompson RG, Patterson BR. Acta mater 1997;45:3653.
[57] Helm EA, Zacharopoulos N, Srolovitz DJ. Acta mater 1998;46:953.
[58] Ono N, Kimura K, Watanabe T. Acta mater 1999;47:1007.
[59] Weygand D, Bréchet Y, Lépinoux J. Mater Sci Eng A 2000;A292:34.
[60] Kazaryan A, Wang Y, Dregia SA, Patton BR. Phys Rev B 2000;61:14275.
[61] Kazaryan A, Wang Y, Dregia SA, Patton BR. Phys Rev B 2001;63:184102.
[62] Miodownik MA, Holm EA, Hassold GN. In: Gottstein G, Molodov D, editors. Recrystallization and Grain Growth, Vol. 1. Berlin: Springer-Verlag; 2001. p. 347–52.
[63] Steinbach I, Apel M, Schaffnit P. In: Gottstein G, Molodov D, editors. Recrystallization and Grain Growth, 1. Berlin: Springer-Verlag; 2001. p. 283–9.
[64] Smith CS. In: Metal Interfaces. Cleveland, OH: American Society for Metals; 1952. pp. 65–113.
[65] Smith CS. Metall Rev 1964;9:1.
[66] Kurtz SK, Kumar S, Banavar JR, Zhang H. In: Pande CS, Marsh SP, editors. Modelling of Coarsening and Grain Growth. Warrendale, PA: The Minerals, Metals & Materials Society; 1993. p. 167–82.
[67] Williams WM, Smith CS. J Metals 1952;4:755.
[68] Weaire D, Rivier N. Contemp Phys 1984;25:59.
[69] Desch CH. J Inst Metals 1919;22:241.
[70] Hull FC. Mater Sci Tech 1988;4:778.
[71] Liu G, Yu H, Song X, Qin X. Mater Design 2001;22:33.
[72] Liu G, Yu H, Li W. Acta Stereol 1994;13:281.
[73] Monnereau C, Vignes-Adler M. Phys Rev Lett 1998;80:5228.
[74] Meijering JL. Philips Res Rep 1953;8:270.
[75] Weaire D, Glazier JA. Phil Mag Lett 1993;68:363.
[76] In Ref. [28] Miyake plots the steady-state grain-size distribution in weighted form against a weighted scaled grain size; the distribution was converted to unweighted frequency and unweighted scaled grain size for inclusion in Fig. 9.
[77] Xiaoyan S, Guoquan L, Nanju G. Scripta mater 2000;43:355.
[78] Holm EA, Glazier JA, Srolovitz DJ, Grest GS. Phys Rev A 1991;43:2662.
[79] Brakke K. Exper Math 1992;1:141.
[80] Weygand D, Bréchet Y, Lépinoux J. Acta mater 1998;46:6559.
[81] Weygand D, Bréchet Y, Lépinoux J. Interface Sci 1999;7:285.
[82] Fan D, Chen L-Q. Acta mater 1997;45:4145.
[83] Fan D, Chen SP, Chen L-Q. J Mater Res 1999;14:1113.
[84] Adams BL, Olson T. Progr Mater Sci 1998;43:1.
[85] Miodownik M, Godfrey AW, Holm EA, Hughes DA. Acta mater 1999;47:2661.